Title
The Neutral Density Temporal Residual Mean overturning circulation

Authors
Stewart, AL
Thompson, AF

Publication Date
2015-06-01

DOI
10.1016/j.ocemod.2015.03.005

Peer reviewed

The Neutral Density Temporal Residual Mean Overturning Circulation

A. L. Stewart[a], and A. F. Thompson[b]

[a]*Department of Atmospheric and Oceanic Sciences, University of California, Los Angeles, CA 90095, USA*
[b]*Environmental Science and Engineering, California Institute of Technology, 1200 E. California Blvd., Pasadena, CA 91125, USA*

Abstract

Diagnosis of the ocean's overturning circulation is essential to closing global budgets of heat, salt and biogeochemical tracers. This diagnosis is sensitive to the choice of density variable used to distinguish water masses and identify transformations between them. The oceanographic community has adopted neutral density for this purpose because its isopycnal slopes are approximately aligned with neutral slopes, along which ocean flows tend to be confined. At high latitudes there are often no tenable alternatives because potential density varies non-monotonically with depth, regardless of the reference pressure. However, in many applications the use of isoneutral fluxes is impractical due to the high computational cost of calculating neutral density. Consequently neutral density-related diagnostics are typically not available as output from ocean models.

In this article the authors derive a modified Temporal Residual Mean (TRM) approximation to the isoneutral mass fluxes, referred to as the Neutral Density Temporal Residual Mean (NDTRM). The NDTRM may be calculated using quantities that are routinely offered as diagnostic output from ocean models, making it several orders of magnitude faster than explicitly computing isoneutral mass fluxes. The NDTRM is assessed using a process model of the Antarctic continental shelf and slope. The onshore transport of warm Circumpolar Deep Water in the model ocean interior approximately doubles when diagnosed using neutral density, rather than potential density. The NDTRM closely approximates these explicitly-computed isoneutral mass fluxes. The NDTRM also exhibits a much smaller error than the traditional TRM in regions of large isoneutral temperature and salinity gradients, where nonlinearities in the equation of state diabatically modify the neutral density.

Keywords:
Transformed Residual Mean, Neutral Density, Ocean Overturning, Antarctic Circulation

1. Introduction

The meridional overturning circulation (MOC) describes the advective transport of mass, heat, salt, and biogeochemical tracers globally between the major ocean basins (Talley, 2013). The importance of this circulation for climate and biogeochemical cycles has motivated attempts to determine a global overturning streamfunction (*e.g.* Lumpkin and Speer, 2007) and the construction of an array of instruments to continuously monitor the MOC in the North Atlantic (Johns et al., 2011). It is difficult in general to characterize the mean paths of fluid parcels, or "streamlines," in a turbulent flow like the ocean or atmosphere, so there is an ongoing effort to develop accurate methods for estimating the MOC. For example Döös et al. (2012) and Zika et al. (2012) have recently proposed a description of the global MOC using a streamfunction with temperature and salinity as coordinates, in which motion along streamlines correspond directly to water mass transformations.

One case in which it is possible to exactly characterize volume transports is when the fluid is constrained to flow within a stack of non-intersecting material surfaces, a criterion that is approximately satisfied by isopycnals in the ocean. It has long been known that calculating the "Eulerian-mean" MOC, *i.e.* using the time- and zonal-averaged velocity, yields misleading results (Döös and Webb, 1994; Nurser and Lee, 2004a; Hirst et al., 1996). Calculating volume fluxes within isopycnal surfaces yields a much more accurate estimate of the transport, accounting for the "eddy" component of the MOC (Marshall and Radko, 2003; Zika et al., 2013). In principle it is possible to compute the MOC from the isopycnal volume fluxes in any predictive ocean model or reanalysis product. To avoid aliasing this calculation requires output of the model velocities and state variables with a time interval much shorter the typical turnover time of mesoscale eddies (Ballarotta et al., 2013). However, the frequency may be limited by digital storage constraints and the burden of post-processing such a large volume of data. These constraints may be circumvented, and the accuracy of the calculation improved, by computing and averaging the isopycnal fluxes during numerical integration of the model. These fluxes are typically available as output in models that use an isopycnal vertical coordinate (*e.g.* Hallberg and Rhines, 1996), and are also available in some non-isopycnal models like the MIT general circulation model (MITgcm, Marshall et al., 1997b,a).

When neither high-frequency model output nor isopycnal fluxes are available, an alternative approach to computing the MOC is to approximate the isopycnal fluxes using the Transformed Eulerian Mean (TEM, Plumb and Ferrari, 2005; Nurser and Lee, 2004b) or Temporal Residual Mean (TRM, McDougall and McIntosh, 1996, 2001). At leading order in the isopycnal fluctuations, the TEM/TRM streamfunctions may be computed solely from the averages of the velocity, the density,

and the product of the velocity and the density (Wolfe, 2014). They therefore incur a much smaller computational cost than directly calculating the fluxes between isopycnal surfaces.

The volume fluxes calculated between isopycnal surfaces will depend upon the choice of density variable. Parcels of ocean water are strongly constrained to follow so-called neutral surfaces, as parcels moving along these surfaces feel no buoyant restoring forces (McDougall, 1987). It is therefore desirable that the isopycnal slopes of the chosen density variable should coincide with neutral slopes (Eden and Willebrand, 1999; McDougall and Jackett, 2005a). Mathematically, neutral surfaces are locally perpendicular to the vector $\boldsymbol{A}$, where

$$\boldsymbol{A} = \beta \nabla S - \alpha \nabla \theta. \tag{1}$$

Here S is the (practical) salinity, θ is the potential temperature, β is the saline contraction coefficient, and α is the thermal expansion coefficient. Neutral surfaces are in fact only well-defined if $\boldsymbol{A}$ has zero helicity, *i.e.* $\boldsymbol{A} \cdot \nabla \times \boldsymbol{A} = 0$ (McDougall, 1987). The helicity of $\boldsymbol{A}$ is generally non-zero due to the nonlinearity of the equation of state for seawater. However, the helicity does tend to be small because the ocean spans a relatively small volume in temperature/salinity/pressure space (McDougall and Jackett, 2007), so for practical purposes an approximate set of neutral surfaces can be constructed.

There are several possible candidates for the density variable that should be used to define isopycnal fluxes. Potential density carries the benefit of being materially conserved away from regions of direct heating or salt forcing, except due to diffusion of temperature and salinity. However, the slopes of potential density surfaces can differ substantially from neutral slopes (McDougall, 1987). This is most pronounced at high latitudes, where potential density may no longer vary monotonically with depth; in such regions, using potential density to compute isopycnal fluxes would result in a substantial loss of information. de Szoeke et al. (2000) constructed an "orthobaric density", by empirically removing the dependence of *in situ* density. However, the corresponding isopycnal slopes still differ substantially from neutral slopes, and orthobaric density also varies non-monotonically with depth in some regions (McDougall and Jackett, 2005a). Jackett and McDougall (1997) proposed a "neutral density" variable γ that is constructed to be constant along approximate neutral surfaces. This construction should ensure monotonicity with depth, though neutral density is only quasi-materially conserved; the nonlinearity of the equation of state precludes the existence of any density variable that is both isoneutral and materially conserved (McDougall and Jackett, 2005b).

Using neutral density to compute the MOC provides an accurate representation of the overturning circulation at all ocean depths, in contrast to potential density (Hirst et al., 1996). However this also magnifies the difficulties associated with calculating isopycnal fluxes, described above, due to the computational expense incurred in calculating the neutral density at many time intervals. Consequently there are currently no ocean models that maintain neutral density as a state variable, offer neutral density as an output product, nor compute mass/volume fluxes between neutral density surfaces. Thus it is not even possible to compute a TEM or TRM streamfunction based on neutral density, as this requires the average of the product of velocity and density $\overline{\boldsymbol{u}\gamma}$. In principle the neutral density and isopycnal volume fluxes could be computed during model integration, or during post-processing from high-frequency model output. However, we will show in §3–4 that the computational cost of calculating neutral density makes such approaches inefficient, especially if applied to global models running at eddy-permitting resolution or higher.

In this paper we propose an efficient method of approximating volume fluxes between neutral density surfaces using a modified TRM that uses only quantities typically available as output from z-coordinate and terrain-following ocean models (*e.g.* Marshall et al., 1997b,a; Haidvogel et al., 2008). More precisely, we assume that the time-mean salinity $\overline{S}$, potential temperature $\overline{\theta}$ and pressure $\overline{p}$ are available, along with the time-mean of the product of the velocity and state variables, *e.g.* $\overline{\boldsymbol{u}\theta}$. This approximate TRM streamfunction, which we refer to as the Neutral Density Temporal Residual Mean (NDTRM) is derived in §2. Then in §3 we test the accuracy of the NDTRM using a process model of the Antarctic continental shelf and slope. Finally, in §4 we discuss our findings and provide concluding remarks.

2. Derivation of the Neutral Density Temporal Residual Mean (NDTRM) streamfunction

2.1. Volume fluxes within neutral density layers

In the interest of a self-contained derivation, we begin with a brief review of McIntosh and McDougall (1996) and McDougall and McIntosh (2001), who derive expressions for the TRM using neutral density as a state variable. We restrict our attention to a Cartesian geometry to simplify our presentation, defining the overbar $\overline{\bullet}$ as a time average over many eddy rotation timescales in a statistically steady state.

Consider a neutral surface $\gamma = \gamma_0$ at a lateral position (x_0, y_0). The depth of the neutral surface is $z = z_0(\gamma_0, t)$. The overturning streamfunction is defined as the lateral volume flux between $z = z_0$ and the ocean surface (*e.g.* Döös and Webb, 1994), which for simplicity we regard as a rigid lid at $z = 0$,

$$\boldsymbol{\Psi}(x_0, y_0, \gamma_0) = \overline{\int_{z=z_0(\gamma_0)}^{z=0} \boldsymbol{u} \, \mathrm{d}z}. \tag{2}$$

Here $\boldsymbol{u} = (u, v)$ is the horizontal velocity vector. Note that $\boldsymbol{\Psi}$ is a function of lateral position and neutral density: vertical gradients in this streamfunction correspond to lateral velocities within density classes, whilst lateral gradients correspond to diapycnal fluxes.

We proceed under the assumption that deviations of the isopycnal depth z_0 from the mean are small compared to the ocean depth, measured by $\varepsilon \sim z_0'/H \ll 1$. We similarly assume that the perturbations of the velocity, potential temperature, salinity and neutral density are small relative to vertical changes in their respective means, *e.g.* $\gamma'/\overline{\gamma}_z H = O(\varepsilon)$. This

holds if such deviations are associated with the eddy-induced vertical heaving of the isopycnals. We may then expand (2) via a Taylor expansion[1],

$$\begin{aligned}\boldsymbol{\Psi} &= \overline{\int_{\overline{z_0}}^{0} \boldsymbol{u}\,\mathrm{d}z} + \overline{\int_{\overline{z_0}+z_0'}^{\overline{z_0}} \boldsymbol{u}\,\mathrm{d}z} \\ &= \int_{\overline{z_0}}^{0} \overline{\boldsymbol{u}}\,\mathrm{d}z + \overline{\int_{\overline{z_0}+z_0'}^{\overline{z_0}} \left\{\boldsymbol{u}(\overline{z_0}) + (z-\overline{z_0})\boldsymbol{u}_z(\overline{z_0}) + O\left((z-\overline{z_0})^2\right)\right\}\mathrm{d}z} \\ &= \int_{\overline{z_0}}^{0} \overline{\boldsymbol{u}}\,\mathrm{d}z - \overline{\boldsymbol{u}(\overline{z_0})z_0' - \tfrac{1}{2}{z_0'}^2\boldsymbol{u}_z(\overline{z_0})} + O\left(\varepsilon^3\right) \\ &= \int_{\overline{z_0}}^{0} \overline{\boldsymbol{u}}\,\mathrm{d}z - \overline{\boldsymbol{u}'(\overline{z_0})z_0'} - \tfrac{1}{2}\overline{\boldsymbol{u}}_z(\overline{z_0})\overline{{z_0'}^2} + O\left(\varepsilon^3\right). \quad (3)\end{aligned}$$

Equation (3) gives an approximation to the lateral volume flux above the isopycnal $z = z_0$ in terms of quantities evaluated at the mean isopycnal depth $z = \overline{z_0}$. The first term in (3) is the flux associated with the mean velocity $\overline{v}$ above the mean isopycnal depth $z = \overline{z_0}$. The second term accounts for net volume fluxes associated with correlations between the velocity and isopycnal depth: if isopycnal depth and velocity perturbations tend to occur together, $\overline{z_0'v'} \neq 0$ then there is on average a net lateral transport associated with those perturbations. The third term accounts for variations in the transport associated with the mean velocity shear: if the velocity is positively sheared then the mean lateral transport anomaly associated with an upward isopycnal displacement is smaller than the opposing transport associated with downward displacements.

McIntosh and McDougall (1996) decompose (3) as

$$\boldsymbol{\Psi}(y_0, \overline{z_0}) = \overline{\boldsymbol{\Psi}} + \boldsymbol{\Psi}^\star, \quad (4a)$$

$$\overline{\boldsymbol{\Psi}} = \int_{\overline{z_0}}^{0} \overline{\boldsymbol{u}}\,\mathrm{d}z, \quad (4b)$$

$$\boldsymbol{\Psi}^\star = -\overline{\boldsymbol{u}'(\overline{z_0})z_0'} - \tfrac{1}{2}\overline{\boldsymbol{u}}_z(\overline{z_0})\,\overline{{z_0'}^2} + O\left(\varepsilon^3\right), \quad (4c)$$

where $\overline{\boldsymbol{\Psi}}$ and $\boldsymbol{\Psi}^\star$ are the mean and eddy streamfunctions respectively. They go on to express z_0' as a function of the mean and perturbation densities ($\overline{\gamma}$,γ') at depth $z = \overline{z_0}$. However, no ocean model currently offers neutral density-related output due to the high cost of computing γ. In §2.2 we instead relate z_0' to the perturbation temperature θ', salinity S' and pressure p', which ocean models must typically compute at every time step in order to solve the equations of motion, and are therefore available at a low computational cost.

Note that the mean density at the mean isopycnal depth $\overline{\gamma}(\overline{z_0})$ may differ from the density γ_0 on the isopycnal $z = z_0(\gamma_0)$ (McDougall and McIntosh, 1996). To obtain the latter we pose a Taylor expansion of the density about the mean isopycnal depth,

$$\gamma_0 = \gamma(\overline{z_0} + z_0') = \gamma(\overline{z_0}) + z_0'\gamma_z(\overline{z_0}) + \tfrac{1}{2}{z_0'}^2\gamma_{zz}(\overline{z_0}) + O\left(\varepsilon^3\right). \quad (5)$$

[1]Formally such asymptotic approximations should be made in dimensionless variables. Throughout the manuscript we retain dimensional variables for clarity and for consistency with previous derivations of the TRM (McIntosh and McDougall, 1996; McDougall and McIntosh, 2001; Nurser and Lee, 2004a,b; Wolfe, 2014).

For consistency with (4c), we wish to relate $\gamma_0(z_0)$ to the isopycnal depth perturbation z_0'. We first take the average of (5),

$$\gamma_0 = \overline{\gamma}(\overline{z_0}) + \overline{z_0'\gamma_z'(\overline{z_0})} + \tfrac{1}{2}\overline{{z_0'}^2}\overline{\gamma}_{zz}(\overline{z_0}) + O\left(\varepsilon^3\right). \quad (6)$$

Subtracting (6) from (5) yields an expression for the perturbation neutral density γ',

$$\gamma'(\overline{z_0}) = -z_0'\overline{\gamma}_z(\overline{z_0}) + O\left(\varepsilon^2\right). \quad (7)$$

Finally, substituting (7) into (6) yields

$$\gamma_0 = \overline{\gamma}(\overline{z_0}) - \frac{\partial}{\partial z}\left(\tfrac{1}{2}\overline{{z_0'}^2}\overline{\gamma}_z\right) + O\left(\varepsilon^3\right). \quad (8)$$

Here we have expressed γ_0 as a function of z_0' because our approximation of the neutral relation in §2.2 yields an expression for z_0', rather than the density perturbation γ', in terms of the temperature and salinity perturbations θ' and S'.

2.2. The neutral relation

The eddy streamfunction (4c) requires evaluation of correlations between the isopycnal depth and velocity perturbations (z_0' and $\boldsymbol{u}'$), or alternatively the density and velocity perturbations (γ' and $\boldsymbol{u}'$) (McIntosh and McDougall, 1996). However, neither z_0' nor γ' are typically offered as ocean model output due to the high cost of computing neutral density. Instead we employ the neutral relation (Jackett and McDougall, 1997) to relate z_0' directly to the hydrographic perturbations (θ',S',p'), which are readily available as ocean model output.

We begin by writing the neutral relation (1) in the form (McDougall, 1987)

$$\beta\nabla_n S = \alpha\nabla_n\theta, \quad (9)$$

where ∇_n is the horizontal gradient operator within the neutral surface. Equation (9) may be derived by taking the dot product of $\boldsymbol{A}$ with vectors tangent to the neutral surface and lying in the x/z and y/z planes respectively. Neutral density is defined with respect to a 4° grid of reference casts, distributed throughout the world ocean (Jackett and McDougall, 1997). The neutral density at any given parcel of ocean water may be determined by finding its isoneutral depth on a nearby reference cast: the neutral density assigned to this depth on the reference cast defines the neutral density of the parcel. In practice the water properties between the parcel and the reference cast may not be available, so an approximate, integrated form of (9) is used. This method is used to determine the parcel's neutral density from each of the four neighboring casts, which are then combined via a weighted average (Jackett and McDougall, 1997). In this subsection and the next we will relate z_0' to the hydrographic perturbations (θ',S',p') with regard to a single neighboring reference cast. However, our calculation of the eddy streamfunction (4c) employs a weighted average over the four nearest reference casts, as explained below.

Consider an arbitrary fluid parcel that lies always on the density surface $\gamma = \gamma_0$, with lateral position (x_0, y_0). At this point, the salinity, potential temperature and pressure are denoted $S_0(\gamma_0, t)$, $\theta_0(\gamma_0, t)$ and $p_0(\gamma_0, t)$ respectively. Let (x_c, y_c)

be the lateral position of a neighboring reference cast. By definition, the parcel is always isoneutral to the depth z_c on the reference cast that has an assigned neutral density of γ_0. We define the salinity, potential temperature and pressure at (x_c, y_c, z_c) as S_c, θ_c and p_c respectively. Integrating (9) along any isoneutral path that connects the parcel and the reference cast, we obtain

$$\int_{l_0}^{l_c} \beta \frac{\partial S}{\partial l}\, \mathrm{d}l = \int_{l_0}^{l_c} \alpha \frac{\partial \theta}{\partial l}\, \mathrm{d}l. \tag{10}$$

Here l is an along-path coordinate, in which l_0 and l_c are the positions of the parcel and the reference cast.

We now approximate (10) by posing a Taylor expansion of the saline contraction and thermal expansion coefficients, *e.g.*

$$\alpha(S, \theta, p) = \alpha_m + (S - S_m)\frac{\partial \alpha_m}{\partial S_m} + (\theta - \theta_m)\frac{\partial \alpha_m}{\partial \theta_m} + (p - p_m)\frac{\partial \alpha_m}{\partial p_m} + O\left(\Delta^2\right). \tag{11}$$

Here the Taylor expansion has been performed about the mid-values of the salinity, potential temperature, and pressure, defined as

$$S_m = \frac{S_0 + S_c}{2}, \quad \theta_m = \frac{\theta_0 + \theta_c}{2}, \quad p_m = \frac{p_0 + p_c}{2}. \tag{12}$$

We have abbreviated $\beta_m = \beta(S_m, \theta_m, p_m)$ and $\alpha_m = \alpha(S_m, \theta_m, p_m)$ for notational convenience. We also use the shorthand notation $\partial\beta_m/\partial S_m \equiv \partial\beta/\partial S(S_m, \theta_m, p_m)$ for partial derivatives. The small parameter Δ measures deviations of the S, θ and p from their midpoint values along the neutral path. One definition for this parameter is the ratio of the parcel-to-cast distance to a dynamical lengthscale L that characterizes lateral property variations, $\Delta = (l_c - l_0)/L \ll 1$, though other definitions could be constructed from (11). In Appendix A we show that (11) may be used to reduce the integrated neutral relation (10) to a direct relationship between the parcel and cast properties,

$$(S_c - S_0)\beta_m - (\theta_c - \theta_0)\alpha_m = O\left(\Delta^3\right). \tag{13}$$

Jackett and McDougall (1997) derive (13) under the assumption that the pressure and potential temperature covary linearly along the neutral path, though they state that in general the error is quadratic in the perturbation terms. In Appendix A we show that in fact the error in (13) is always cubic.

2.3. Neutral surface depth perturbations

We now use (13) to relate the isopycnal depth perturbations z_0' to the perturbation salinity S_0', potential temperature θ_0' and pressure p_0'. First, we pose a double Taylor expansion of the isopycnal salinity S_0 in terms of the isopycnal depth perturbation z_0' and the salinity perturbation at the mean isopycnal depth $S_0'(\overline{z_0}, t)$,

$$\begin{aligned} S_0(\gamma_0, t) &= S(z_0(\gamma_0, t), t) = S(\overline{z_0} + z_0', t) \\ &= S(\overline{z_0}, t) + z_0' S_z(\overline{z_0}, t) + O\left(\varepsilon^2\right) \\ &= \overline{S}(\overline{z_0}) + S'(\overline{z_0}, t) + z_0'\overline{S}_z + O\left(\varepsilon^2\right). \end{aligned} \tag{14}$$

In (14) and hereafter all quantities are implicitly evaluated at the lateral parcel position (x_0, y_0). Taking the mean of (14) relates the mean isopycnal salinity to the mean salinity at the mean isopycnal depth,

$$\overline{S_0(\gamma_0, t)} = \overline{S} + O\left(\varepsilon^2\right), \tag{15}$$

where again we use the shorthand $\overline{S} \equiv \overline{S}(\overline{z_0})$. Analogous results to (14) and (15) hold for the potential temperature θ and pressure p.

Second, we pose a Taylor expansion of the saline contraction and thermal expansion coefficients evaluated at the midpoint properties between the parcel and reference cast. For example, using (14) we may expand α_m as

$$\begin{aligned} \alpha_m &= \alpha\left[\tfrac{1}{2}(S_0 + S_c), \tfrac{1}{2}(\theta_0 + \theta_c), \tfrac{1}{2}(p_0 + p_c)\right] \\ &= \alpha\Big[\tfrac{1}{2}\left(\overline{S} + S' + z_0'\overline{S}_z + S_c\right), \tfrac{1}{2}\left(\overline{\theta} + \theta' + z_0'\overline{\theta}_z + \theta_c\right), \\ &\qquad \tfrac{1}{2}\left(\overline{p} + p' + z_0'\overline{p}_z + p_c\right)\Big] + O\left(\varepsilon^2\right) \\ &= \overline{\alpha}_m + \tfrac{1}{2}\left(S' + z_0'\overline{S}_z\right)\frac{\partial \overline{\alpha}_m}{\partial \overline{S}_m} + \tfrac{1}{2}\left(\theta' + z_0'\overline{\theta}_z\right)\frac{\partial \overline{\alpha}_m}{\partial \overline{\theta}_m} \\ &\qquad + \tfrac{1}{2}\left(p' + z_0'\overline{p}_z\right)\frac{\partial \overline{\alpha}_m}{\partial \overline{p}_m} + O\left(\varepsilon^2\right). \end{aligned} \tag{16}$$

Here we denote the mean midpoint salinity, potential temperature and pressure as

$$\overline{S}_m \equiv \frac{\overline{S} + S_c}{2}, \quad \overline{\theta}_m \equiv \frac{\overline{\theta} + \theta_c}{2}, \quad \overline{p}_m \equiv \frac{\overline{p} + p_c}{2}, \tag{17}$$

respectively. Note that (17) defines the midpoint of the mean parcel and cast properties, rather than the mean of the midpoint parcel and cast properties (12), though from (15) these quantities are identical up to $O(\varepsilon^2)$, *e.g.* $\overline{S}_m = \overline{S_m(\gamma_0, t)} + O(\varepsilon^2)$. We use a similar shorthand for the saline contraction and thermal expansion coefficients evaluated at the midpoint of the mean parcel and cast properties

$$\overline{\beta}_m \equiv \beta\left(\overline{S}_m, \overline{\theta}_m, \overline{p}_m\right), \quad \overline{\alpha}_m \equiv \alpha\left(\overline{S}_m, \overline{\theta}_m, \overline{p}_m\right). \tag{18}$$

We use the shorthand notation $\partial\overline{\beta}_m/\partial\overline{S}_m \equiv \partial\beta/\partial S(\overline{S}_m, \overline{\theta}_m, \overline{p}_m)$ for partial derivatives.

Finally, we substitute (14) (and equivalent expressions for θ and p) and (16) (and the equivalent expression for β_m) into (13).

Neglecting terms of $O(\varepsilon^2)$ and higher and rearranging yields

$$
\begin{aligned}
z_0' \Big\{ & -\overline{S}_z\overline{\beta}_m + \overline{\theta}_z\overline{\alpha}_m \\
& + \left(S_c - \overline{S}\right)\left[\tfrac{1}{2}\overline{S}_z\frac{\partial\overline{\beta}_m}{\partial\overline{S}_m} + \tfrac{1}{2}\overline{\theta}_z\frac{\partial\overline{\beta}_m}{\partial\overline{\theta}_m} + \tfrac{1}{2}\overline{p}_z\frac{\partial\overline{\beta}_m}{\partial\overline{p}_m}\right] \\
& - \left(\theta_c - \overline{\theta}\right)\left[\tfrac{1}{2}\overline{S}_z\frac{\partial\overline{\alpha}_m}{\partial\overline{S}_m} + \tfrac{1}{2}\overline{\theta}_z\frac{\partial\overline{\alpha}_m}{\partial\overline{\theta}_m} + \tfrac{1}{2}\overline{p}_z\frac{\partial\overline{\alpha}_m}{\partial\overline{p}_m}\right] \Big\} \\
= -\Big\{ & -S'\overline{\beta}_m + \theta'\overline{\alpha}_m \\
& + \left(S_c - \overline{S}\right)\left[\tfrac{1}{2}S'\frac{\partial\overline{\beta}_m}{\partial\overline{S}_m} + \tfrac{1}{2}\theta'\frac{\partial\overline{\beta}_m}{\partial\overline{\theta}_m} + \tfrac{1}{2}p'\frac{\partial\overline{\beta}_m}{\partial\overline{p}_m}\right] \\
& - \left(\theta_c - \overline{\theta}\right)\left[\tfrac{1}{2}S'\frac{\partial\overline{\alpha}_m}{\partial\overline{S}_m} + \tfrac{1}{2}\theta'\frac{\partial\overline{\alpha}_m}{\partial\overline{\theta}_m} + \tfrac{1}{2}p'\frac{\partial\overline{\alpha}_m}{\partial\overline{p}_m}\right] \Big\} \\
& + O\left(\Delta^3, \varepsilon^2\right), \qquad (19)
\end{aligned}
$$

where implicitly all quantities are evaluated at $z = \overline{z_0}$. Using (19), the eddy streamfunction (4c) can be expressed entirely in terms of averaged products that are readily available as output from ocean models, namely $\overline{\boldsymbol{u}'S'}$, $\overline{\boldsymbol{u}'\theta'}$, $\overline{\boldsymbol{u}'p'}$, $\overline{S'^2}$, $\overline{\theta'^2}$, $\overline{p'^2}$, $\overline{S'\theta'}$, $\overline{S'p'}$, and $\overline{\theta'p'}$. We derived (19) based on a single neighboring reference cast, but in practice one would compute the eddy streamfunction (4c) using a weighted average over the four neighboring reference casts (Jackett and McDougall, 1997). We provide explicit expressions for the eddy streamfunction in Appendix B.1.

The cast properties are strictly functions of the neutral density surface γ_0, *e.g.* $\theta_c = \theta_c(\gamma_0)$. In practice these are determined approximately via (5)

$$
\begin{aligned}
\theta_c(\gamma_0) &= \theta_c\left(\gamma(\overline{z_0}) + z_0'\gamma_z(\overline{z_0}) + O\left(\varepsilon^2\right)\right) \\
&= \theta_c\left(\overline{\gamma}(\overline{z_0}) + \gamma'(\overline{z_0}) + z_0'\overline{\gamma}_z(\overline{z_0}) + O\left(\varepsilon^2\right)\right) \\
&= \theta_c(\overline{\gamma}(\overline{z_0})) + \left[\gamma'(\overline{z_0}) + z_0'\overline{\gamma}_z(\overline{z_0})\right]\frac{\partial\theta_c}{\partial\gamma_0}(\overline{\gamma}(\overline{z_0})) + O\left(\varepsilon^2\right) \\
\implies \theta_c(\gamma_0) &= \theta_c(\overline{\gamma}(\overline{z_0})) + O\left(\varepsilon^2\right), \qquad (20)
\end{aligned}
$$

where the final equation follows from taking an average of both sides of the equality, and noting that $\overline{\theta_c(\gamma_0)} = \theta_c(\gamma_0)$.

2.4. The Boussinesq case

Most ocean models (*e.g.* Hallberg and Rhines, 1996; Marshall et al., 1997a; Shchepetkin and McWilliams, 2005) employ the Boussinesq approximation for computational simplicity, in which the equation of state is simplified to prescribe the density as a function of salinity S, potential temperature θ, and hydrostatic pressure via the depth z. Following a similar derivation as above, in this case the neutral surface depth perturbations are given by

$$
\begin{aligned}
z_0' \Big\{ & -\overline{S}_z\overline{\beta}_m + \overline{\theta}_z\overline{\alpha}_m \\
& + \left(S_c - \overline{S}\right)\left[\tfrac{1}{2}\overline{S}_z\frac{\partial\overline{\beta}_m}{\partial\overline{S}_m} + \tfrac{1}{2}\overline{\theta}_z\frac{\partial\overline{\beta}_m}{\partial\overline{\theta}_m} + \tfrac{1}{2}\frac{\partial\overline{\beta}_m}{\partial\overline{z}_m}\right] \\
& - \left(\theta_c - \overline{\theta}\right)\left[\tfrac{1}{2}\overline{S}_z\frac{\partial\overline{\alpha}_m}{\partial\overline{S}_m} + \tfrac{1}{2}\overline{\theta}_z\frac{\partial\overline{\alpha}_m}{\partial\overline{\theta}_m} + \tfrac{1}{2}\frac{\partial\overline{\alpha}_m}{\partial\overline{z}_m}\right] \Big\} \\
= -\Big\{ & -S'\overline{\beta}_m + \theta'\overline{\alpha}_m \\
& + \left(S_c - \overline{S}\right)\left[\tfrac{1}{2}S'\frac{\partial\overline{\beta}_m}{\partial\overline{S}_m} + \tfrac{1}{2}\theta'\frac{\partial\overline{\beta}_m}{\partial\overline{\theta}_m}\right] \\
& - \left(\theta_c - \overline{\theta}\right)\left[\tfrac{1}{2}S'\frac{\partial\overline{\alpha}_m}{\partial\overline{S}_m} + \tfrac{1}{2}\theta'\frac{\partial\overline{\alpha}_m}{\partial\overline{\theta}_m}\right] \Big\} \\
& + O\left(\Delta^3, \varepsilon^2\right). \qquad (21)
\end{aligned}
$$

This modifies the eddy streamfunction $\boldsymbol{\Psi}^\star$, the explicit form for which is discussed in Appendix B.2.

We have found that little accuracy is lost (see §3) if the $O(\varepsilon\Delta)$ terms are neglected from (21), namely those proportional to derivatives of $\overline{\beta}_m$ and $\overline{\alpha}_m$. Under this approximation the neutral surface depth perturbation is given by a much simpler expression,

$$
z_0' = -\frac{S'\overline{\beta}_m - \theta'\overline{\alpha}_m}{\overline{S}_z\overline{\beta}_m - \overline{\theta}_z\overline{\alpha}_m} + O\left(\Delta^3, \varepsilon^2, \varepsilon\Delta\right). \qquad (22)
$$

This simplified form is somewhat easier to interpret in physical terms: the denominator of (22) resembles an expression for density stratification N^2, whilst the numerator approximately measures changes in density associated with fluctuations in salinity and potential temperature. Importantly, the saline contraction and thermal expansion coefficients are evaluated midway between the parcel and the cast. This crudely approximates the fact that density variations of the parcel are determined by temperature and salinity perturbations with respect to the integrated saline contraction and thermal expansion coefficients

Table 1: Definitions of the Boussinesq TRM streamfunctions discussed in this paper. The second column provides equation numbers corresponding to our various approximations of the isopycnal depth perturbation z_0'. Explicit forms for the eddy components of these TRM streamfunctions are given in Appendix B. The third column provides equation numbers for the equivalent TEM forms of the eddy streamfunctions, which are compared in §3. The fourth column provides the formal accuracy of each streamfunction; ε and Δ are defined in §2 below (2) and (12) respectively.

Streamfunction	Def. of z_0'	TEM $\psi^\star$	Accuracy
$\boldsymbol{\Psi}^{(\sigma)}_{\text{TRM}}$	(25)	(B.11)	$O(\varepsilon^3)$
$\boldsymbol{\Psi}^{(\gamma)}_{\text{TRM}}$	(24)	(B.12)	$O(\varepsilon^3)$
$\boldsymbol{\Psi}^{(\gamma)}_{\text{NDTRM0}}$	(23)	(B.10)	$O\left(\varepsilon\Delta^2, \varepsilon^3, \varepsilon^2\Delta\right)$
$\boldsymbol{\Psi}^{(\gamma)}_{\text{NDTRM1}}$	(22)	(B.9)	$O\left(\varepsilon\Delta^3, \varepsilon^3, \varepsilon^2\Delta\right)$
$\boldsymbol{\Psi}^{(\gamma)}_{\text{NDTRM2}}$	(21)	(B.8)	$O\left(\varepsilon\Delta^3, \varepsilon^3\right)$

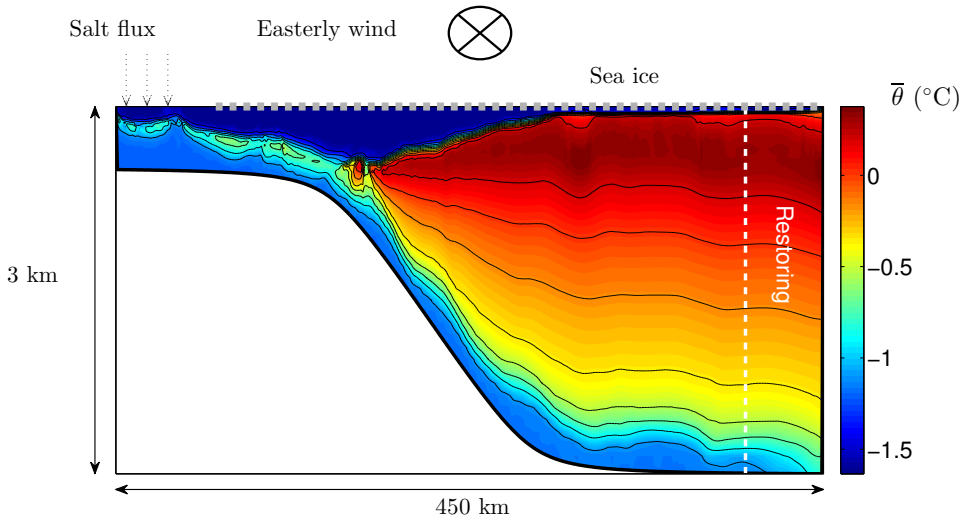

Figure 1: Schematic of the model-setup for our Antarctic shelf/slope test case. Contours show a snapshot of the daily-averaged potential temperature field.

along neutral paths, rather than their local values. We can obtain an expression for z_0' that depends entirely on local quantities by taking the approximation a step further,

$$z_0' = -\frac{S'\overline{\beta} - \theta'\overline{\alpha}}{\overline{S}_z\overline{\beta} - \overline{\theta}_z\overline{\alpha}} + O\left(\Delta^2, \varepsilon^2, \varepsilon\Delta\right). \tag{23}$$

Here $\overline{\alpha}$ and $\overline{\beta}$ are shorthands for $\alpha(\overline{S}, \overline{\theta}, \overline{p})$ and $\beta(\overline{S}, \overline{\theta}, \overline{p})$ respectively. In this case the denominator is exactly proportional to the density stratification, and the numerator is proportional to the variations of locally-referenced potential density with salinity and potential temperature. The eddy streamfunctions corresponding to both (22) and (23) are given in Appendix B.2.

2.5. Traditional TRM isopycnal depth perturbations

For the purpose of comparison, we also provide an expression for the isopycnal depth perturbation z_0' directly in terms of the density perturbation γ', which may be obtained by rearranging (7) as

$$z_0' = -\frac{\gamma'}{\overline{\gamma}_z} + O\left(\varepsilon^2\right). \tag{24}$$

The resulting TRM streamfunction is much simpler than the full NDTRM streamfunction. However, accurate calculation of the product $\overline{\boldsymbol{u}'\gamma'}$ requires the neutral density to be computed everywhere in the domain, a feature not currently available in ocean models, and which imposes a substantial additional computational burden (see §3).

To provide an independent benchmark for the accuracy of the TRM, we employ an analogous expression for z_0' in terms of the potential density perturbation σ',

$$z_0' = -\frac{\sigma'}{\overline{\sigma}_z} + O\left(\varepsilon^2\right). \tag{25}$$

The corresponding TRM streamfunction is given by (B.11). The various approximations to the isopycnal depth perturbation and eddy streamfunction derived in this section are summarized in Table 1.

3. A test case: overturning at the Antarctic margins

In this section we assess the accuracy of our various approximations to the TRM streamfunction, listed in Table 1. We perform this assessment using a process model of the Antarctic continental shelf and slope, a region where the nonlinearities in the equation of state are particularly pronounced (*e.g.* Gill, 1973). To facilitate our analysis and ensure computational efficiency, we simplify the model geometry and physics where possible, but retain sufficient detail to qualitatively reproduce the water mass structure associated with the Antarctic Slope Front (Thompson and Heywood, 2008). Stewart and Thompson (2015) discuss the implications of this model for cross-slope exchange around the Antarctic margins.

3.1. Model configuration

The model configuration is sketched in Figure 1, which shows an instantaneous cross-slope slice of the model's potential temperature field. We used the MIT general circulation model (MITgcm, Marshall et al., 1997b,a) to simulate the flow in a re-entrant channel with a cross-channel width of $L_y = 450\,\text{km}$, an along-channel length $L_x = 400\,\text{km}$, and a depth of 3000 m. The ocean depth shoals to 500 m at the shoreward boundary, as shown in Figure 1, via a continental slope whose dimensions are typical of the Western Weddell Sea. The domain lies on an f-plane with Coriolis parameter $f_0 = -1.31 \times 10^{-4}\,\text{rad}\,\text{s}^{-1}$.

A 50 km-wide strip of the ocean surface at the shoreward edge of the domain is forced by a fixed salt input of $2.5 \times 10^{-3}\,\text{g}\,\text{m}^{-2}\,\text{s}^{-1}$, typical of the brine rejection associated with sea ice formation in coastal polynyas (Tamura et al., 2008). North of this, we impose a steady, piecewise-sinusoidal westward wind stress with a maximum strength of $0.075\,\text{N}\,\text{m}^{-2}$ over the center of the continental slope, representative of conditions around the Antarctic margins (Large and Yeager, 2009). The remainder of the surface interacts thermodynamically with a

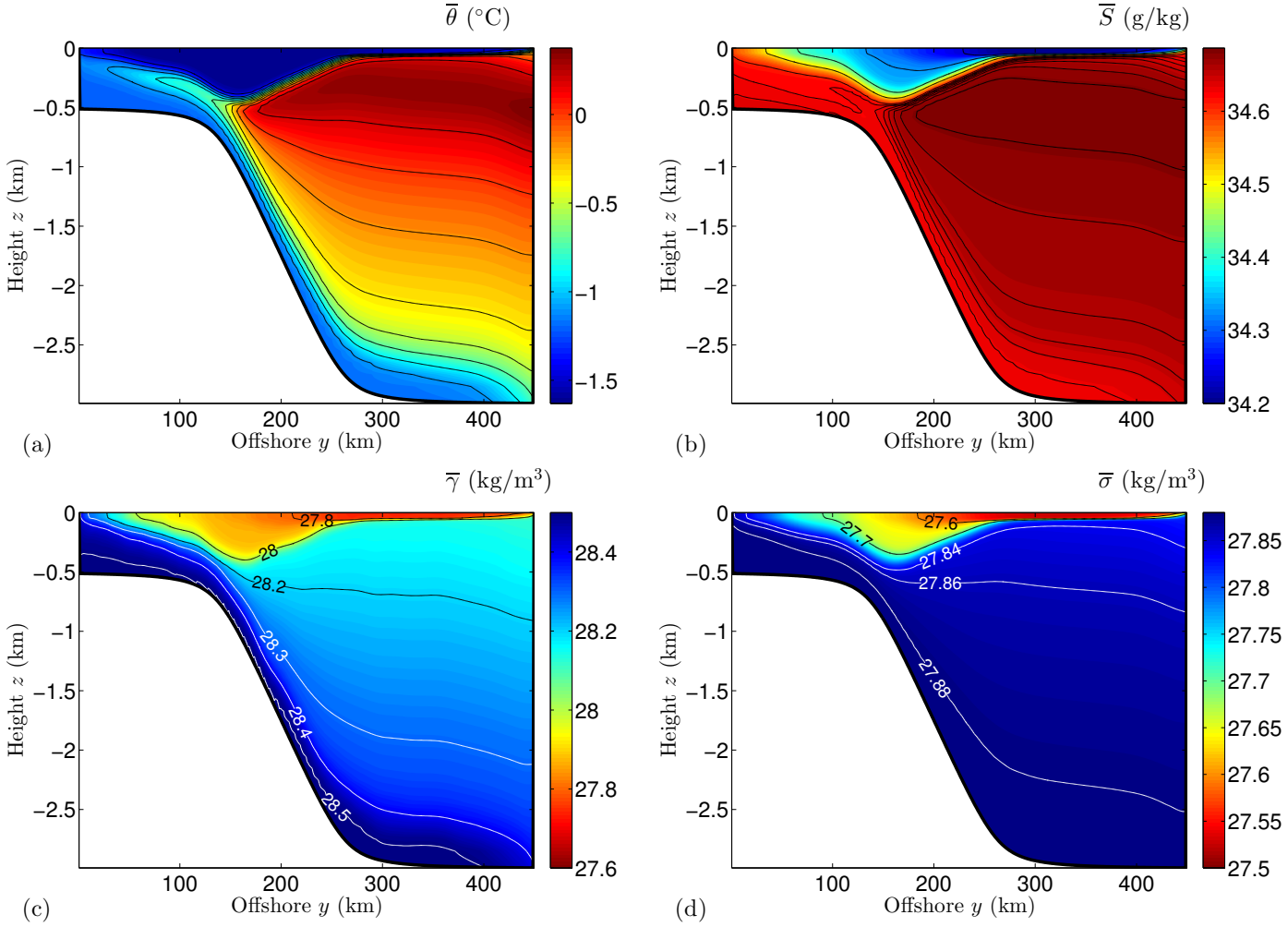

Figure 2: Time- and alongshore-mean (a) potential temperature, (b) salinity, (c) neutral density and (d) potential density referenced to the surface. The time average was taken over 5 years in statistically steady state.

layer of sea ice of fixed width 1 m, which does not itself evolve in response to the ocean below. Thermodynamic exchanges are computed according to a two-equation ice-ocean boundary layer model Schmidt et al. (2004). The offshore boundary is restored to Weddell Sea hydrography (Thompson and Heywood, 2008). The model properties therfore remain close to the hydrography of the real Weddell Sea, and thus the neutral density defined by Jackett and McDougall (1997) accurately quantifies the density stratification. The restoring increases linearly from zero at the edge of the restoring region to a timescale of 56 days at the offshore boundary.

Momentum is extracted at the ocean bed via a linear drag with coefficient $r_b = 1 \times 10^{-3}\,\mathrm{m\,s^{-1}}$. We also extract energy via a lateral Laplacian viscosity of $12\,\mathrm{m^2\,s^{-1}}$, a vertical Laplacian viscosity of $3\times10^{-4}\,\mathrm{m^2\,s^{-1}}$, a dimensionless biharmonic viscosity of 0.1, and dimensionless biharmonic Leith and modified-Leith viscosities (Fox-Kemper and Menemenlis, 2008), both equal to 1. Potential temperature and salinity are subject to vertical diffusion with coefficients of $5 \times 10^{-6}\,\mathrm{m^2\,s^{-1}}$.

The model employs a spatial resolution of 1 km in the horizontal, whilst the vertical grid spacings ranges from 13m at the surface to 100m at the ocean bed. We found that cross-slope transport in the ocean interior was reduced by around 50% when the horizontal resolution was reduced to 2 km, whereas increasing the resolution to 0.5 km did not substantially change the solution. We integrate the momentum equation forward in time using a second-order Adams-Bashforth scheme, while tracers are evolved using the second-order moment advection scheme of Prather (1986), which has been shown to minimize numerical diapycnal diffusion in the MITgcm (Hill et al., 2012). The time step of 179 s was chosen to ensure the advective CFL criterion would be satisfied at all points in space and time. The model was integrated until it reached statistically steady state, as judged from time series of the total and eddy kinetic energies.

In Figure 2 we plot the time- and alongshore-mean potential temperature, salinity, neutral density and potential density in statistically steady state. The model captures the characteristic water mass structure of the Antarctic Slope Front in the western Weddell Sea (Thompson and Heywood, 2008), with the warm, salty layer of Circumpolar Deep Water (CDW) sandwiched be-

tween relatively cold, fresh Antarctic Surface Waters (AASW) and a deep outflow of Antarctic Bottom Water (AABW). We will show that the overturning circulation is more accurately computed using neutral density, shown in Figure 2(c), than potential density, shown in Figure 2(d). In the cross-slope hydrographic data collected by Thompson and Heywood (2008), the potential density always varies non-monotonically with depth somewhere, regardless of the reference level. As a result, computing the isopycnal transports using any potential density would lead to a loss of information. In our model test case it so happens that surface-referenced potential density varies monotonically with depth everywhere, and so can be used to quantify the utility of computing the overturning circulation using neutral density. However, we emphasize that this is a special case: defining the potential density with reference to deeper levels, or modifying the forcing parameters, leads to non-monotonicity in the potential density stratification. We will henceforth refer to surface-referenced potential density simply as the potential density σ.

3.2. Computing the overturning circulation

The purpose of our test case is to assess our various approximations to the TRM against an accurate calculation of the model's isopycnal volume transports. The along-slope symmetry of the model geometry and forcing allow us to simplify this analysis by computing the overturning circulation in the y/z plane only, reinterpreting the averaging operator $\overline{\bullet}$ in §2 as a time- and alongshore-mean and the streamfunctions as only having one component. In realistic ocean geometries this not possible because the properties (S_c, θ_c, p_c) of the nearest reference casts are themselves functions of latitude, longitude and depth. Instead the TRM streamfunction components would need to be computed at all points in space, and then the alongshore-integrated fluxes computed between the time-mean isopycnals. In our case, however, the entire domain lies conceptually along a transect from (61W,67S) to (50.6W,67S), so the cast properties are only functions of y and z.

We define the "exact" cross-slope overturning streamfunctions as follows,

$$\psi^{(\phi)}(y, \overline{z_0}(\phi_0)) = \overline{\int_{z=z_0(\phi_0)}^{0} v \, \mathrm{d}z} \tag{26}$$

where $\phi = \gamma$ or $\phi = \sigma$ for neutral density and potential density respectively. Here $\phi = \phi_0$ defines an arbitrary isopycnal surface, and $z_0(\phi_0)$ and $\overline{z_0}(\phi_0)$ are the instantaneous and mean depths of that isopycnal. For the case of potential density $\phi = \sigma$, we used the MITgcm LAYERS package to compute the mean cross-slope volume fluxes and mean layer thicknesses within 181 discrete density layers spanning the range shown in Figure 2. We used a much finer density increment between the densest layers to account for the larger range of depths spanned by those densities. The mean was calculated by computing the fluxes and layer thicknesses in each density layer at each time step and averaging over time. Such an operation would be prohibitively computationally expensive if attempted with neutral density. Instead we performed the equivalent calculation by computing the neutral density from the daily-averaged potential temperature, salinity, and velocity fields, and computing the fluxes and layer thicknesses within 143 discrete density layers.

To compute the two-dimensional TRM streamfunctions we use the daily-averaged potential temperature θ and salinity S to compute the neutral density γ and potential density σ everywhere in the domain. We combine these quantities with the daily-averaged cross-slope velocity v to compute the mean and correlation terms in the various TRM streamfunctions listed in Table 1. Again, the averaging operator $\overline{\bullet}$ is redefined as an average in time and along the slope, so we consider only the cross-slope component of each streamfunction. These streamfunctions therefore correspond to taking a Transformed Eulerian Mean (TEM, *e.g.* McIntosh and McDougall, 1996), so we denote them with the subscript $_{\mathrm{TEM}}$ to differentiate them from the full, three-dimensional TRM streamfunctions derived in §2. For example,

$$\psi^{\star(\gamma)}_{\mathrm{TEM}}(y_0, \overline{z_0}) = \frac{\overline{v'\gamma'}}{\overline{\gamma}_z}, \tag{27}$$

where $\overline{\gamma}$ is the neutral density averaged over 5 years of daily output and in the along-slope direction, and v' and γ' are the deviations of the daily cross-slope velocity and neutral density from their respective means. Explicit TEM versions of the streamfunctions listed in Table 1 are given in Appendix B.

3.3. Accuracy of the NDTEM/NDTRM

We now directly quantify the error associated with various approximations to the overturning circulation in neutral density layers. For reference, we first consider the TEM approximation to the overturning circulation in potential density layers. Figure 3 panel (a) shows the exact overturning streamfunction $\psi^{(\sigma)}$. The overturning circulation is characterized by a single counter-clockwise cell with sinking on the continental shelf and upwelling in the offshore restoring region. The majority of the onshore transport ($\sim 2/3$) is wind-driven AASW and concentrated close to the surface, whilst the remainder ($\sim 1/3$) is CDW following an interior pathway. All onshore transport is balanced by an outflow of AABW along the ocean bed. Panel (b) shows the pointwise error in the potential density TRM streamfunction $\psi^{(\sigma)}_{\mathrm{TEM}}$. The largest errors are mostly found close to ocean surface and bed, where isopycnals intersect solid boundaries and the integral between the isopycnal depth and the surface in (3) is not well defined (Young, 2012). Away from the boundaries the pointwise errors are very small, less than 5% over most of the domain. The major exception is the continental shelf, where the shallow ocean depth results in the generation of submesoscale flows and relatively large departures of the isopycnal surfaces from their mean depths. This corresponds to a larger value of ε in (4c), and consequently the relative error is around 25% at some points. Below we will show that the error in the cross-slope transport is much smaller than this; to some extent the pointwise errors describe a slight shift in the depth of the overturning cell on the continental shelf.

In panels (c) and (d) of Figure 3 we present analogous plots using streamfunctions based on neutral density. The overturning circulation is qualitatively similar, but somewhat stronger

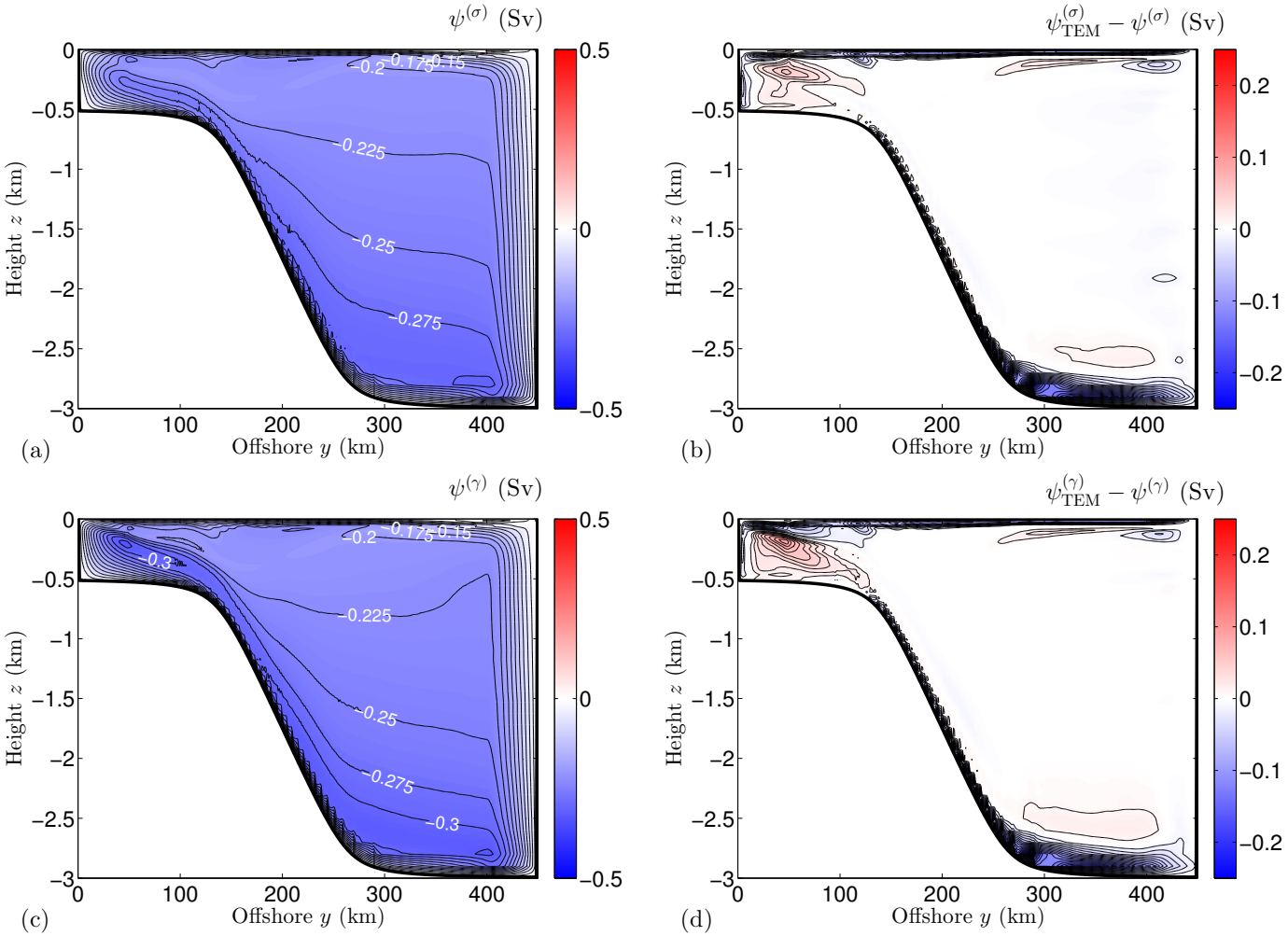

Figure 3: (a) Exact overturning circulation computed within potential density layers via (26) with $\phi = \sigma$ and (b) error associated with the traditional TEM approximation using eddy potential density fluxes, equivalent to (B.11). Here potential density is referenced to the surface. (c,d) Equivalent plots using neutral density-based streamfunctions, *i.e.* using (26) with $\phi = \gamma$ for (c) and (B.12) for (d). In panels (a) and (c) the contour interval is 0.025 Sv, and in panels (b) and (d) the contour interval is 0.01 Sv.

due to an enhancement of the onshore transport of CDW in the ocean interior. Below we will show that the onshore transport of CDW increases by over 50% when volume fluxes are calculated within neutral density layers instead of potential density. This discrepancy is partly due to the fact that the slopes of potential density surfaces differ from neutral slopes. At any point the local neutral slope satisfies

$$\boldsymbol{s}_\gamma = -\frac{\beta(S,\theta,p)\nabla_h S - \alpha(S,\theta,p)\nabla_h\theta}{\beta(S,\theta,p)S_z - \alpha(S,\theta,p)\theta_z}, \tag{28}$$

where $\nabla_h \equiv (\partial_x, \partial_y)$ is the horizontal gradient. In practice the slope of the neutral density surfaces is determined by the approximate neutral relation (13). The slope of the potential density surfaces should satisfy

$$\boldsymbol{s}_\sigma = -\frac{\beta(S,\theta,p_{\mathrm{ref}})\nabla_h S - \alpha(S,\theta,p_{\mathrm{ref}})\nabla_h\theta}{\beta(S,\theta,p_{\mathrm{ref}})S_z - \alpha(S,\theta,p_{\mathrm{ref}})\theta_z}, \tag{29}$$

where p_{ref} is the surface pressure. The saline contraction coefficient β varies weakly with depth, so $\boldsymbol{s}_\gamma$ and $\boldsymbol{s}_\sigma$ differ largely due to the pressure-dependence of the thermal-expansion coefficient α (McDougall, 1987). For our surface-referenced potential density σ, the difference in the slopes is most pronounced close to the ocean bed, where the pressure is much greater than p_{ref}, and in the coldest parts of the domain, where $\partial\alpha/\partial p$ is largest. Thus the enhancement of $\psi^{(\gamma)}$ relative to $\psi^{(\sigma)}$ in Figure 3(a) and (c) is most pronounced in the cold outflow of AABW, close to the ocean bed. The neutral density TEM $\psi^{(\gamma)}_{\mathrm{TEM}}$ is qualitatively similar to the potential density TEM, though the errors on the continental shelf have a maximum magnitude of ~30% in this case.

We now turn our attention to the new streamfunctions derived from the neutral relation in §2. In Figure 4(a) we have reproduced for reference the exact overturning circulation computed from fluxes within neutral density layers. In panels (b–c) we plot successively more accurate approximations $\psi^{(\gamma)}_{\mathrm{NDTEM0}}$, $\psi^{(\gamma)}_{\mathrm{NDTEM1}}$ and $\psi^{(\gamma)}_{\mathrm{NDTEM2}}$ corresponding to approximations (23), (22), and (21) respectively. The lowest-order approximation,

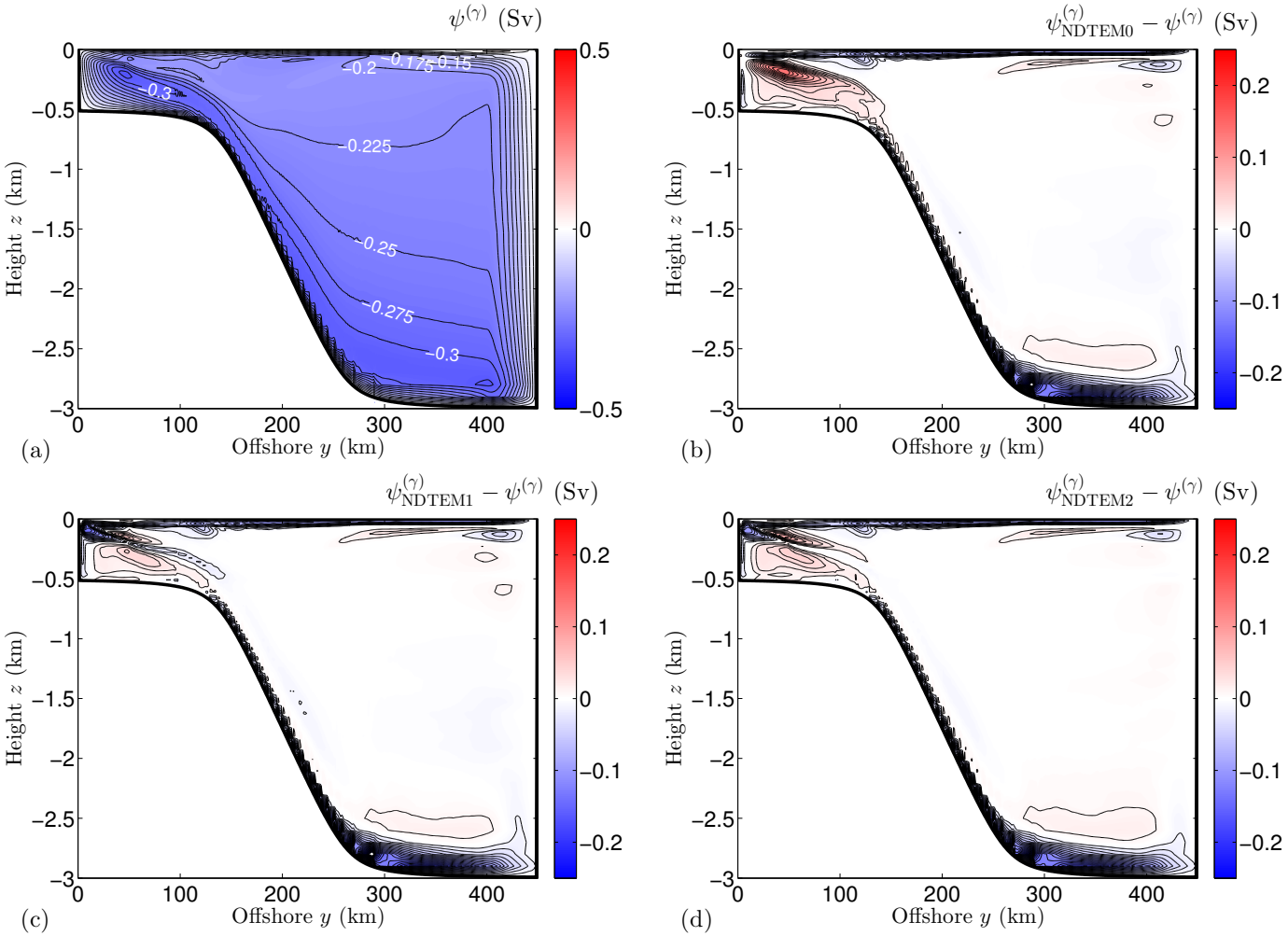

Figure 4: (a) Exact overturning circulation computed within neutral density layers. (b-d) Error in the TEM overturning streamfunctions (B.10), (B.9) and (B.8) calculated using successively more accurate approximations to the isopycnal depth perturbation z'_0, derived from the neutral relation (9) in §2. In panel (a) the contour interval is 0.025 Sv, and in panels (b–d) the contour interval is 0.01 Sv.

$\psi^{(\gamma)}_{\mathrm{NDTEM0}}$, is equivalent to computing the TEM using the locally-referenced potential density, as advocated by McIntosh and McDougall (1996). This is the least accurate approximation, with relative errors close to 50% on the continental shelf. Using the higher-order approximations improves the agreement of the TEM with the exact streamfunction, reducing the typical relative errors in the ocean interior on the continental shelf to around 20%. However, it is unclear whether there is much improvement between $\psi^{(\gamma)}_{\mathrm{NDTEM1}}$ and $\psi^{(\gamma)}_{\mathrm{NDTEM2}}$. The largest relative errors in the ocean interior on the continental shelf actually increase to approximately 33% for $\psi^{(\gamma)}_{\mathrm{NDTEM2}}$, though we note that this measure of the error is particularly sensitive to noise.

3.4. Shoreward water mass transport

The pointwise errors between exact and TEM streamfunctions shown in Figures 3 and 4 can be misleading because a slight shift in the position of a strong overturning circulation can produce a large pointwise error. Arguably a more physically relevant quantity is the cross-slope transport, and in particular the net transport of water masses across the width of the domain. In Figure 5(a) we plot the total shoreward volume transport as a function of offshore position y_0, defined by streamlines that originate at the edge of the restoring region $y = 400\,\mathrm{km}$ and extend continuously to $y = y_0$. By definition this transport increases monotonically with y_0, with some streamlines that originate at $y = 400\,\mathrm{km}$ forming closed loops before they reach the continental shelf, visible in Figure 3 panels (a) and (c).

Figure 3 indicates that switching from potential to neutral density increases the calculated transport in the ocean interior, and thus the transport of warm CDW onto the continental shelf. In Figure 5(b) we therefore also plot the net shoreward CDW transport, defined analogously to the total transport but counting only streamlines that lie within the CDW layer. We define the AASW/CDW boundary as a potential density of $27.84\,\mathrm{kg\,m^{-3}}$ or a neutral density of $28.15\,\mathrm{kg\,m^{-3}}$.

The cross-slope structures of the total and interior shoreward transports, shown in Figures 5(a) and (b) respectively, bear

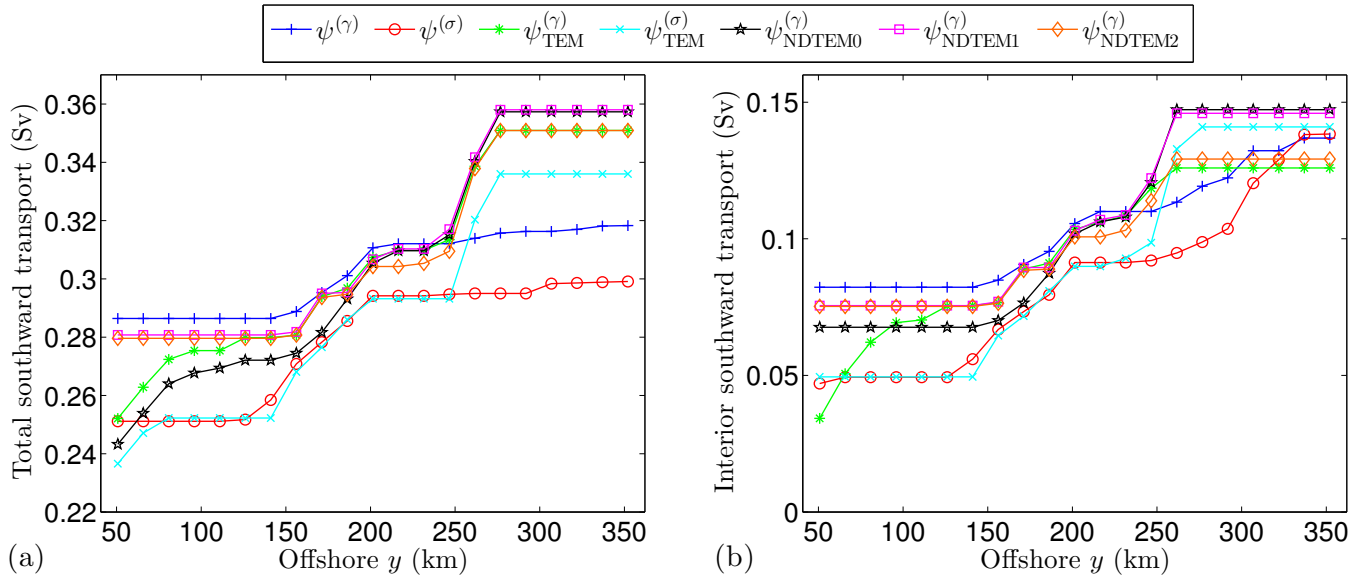

Figure 5: (a) Total shoreward transport and (b) interior shoreward transport as functions of offshore distance, calculated for a range of "exact" and TEM streamfunctions as described in §3.4.

strong resemblance to one another. This implies that most of the discrepancies between the total shoreward transports predicted by the various streamfunctions are associated with the interior CDW transport, rather than the near-surface AASW transport. Although the error between the TEM and exact streamfunctions is relatively small compared to the total shoreward transport, they constitute a much larger fraction of the interior transport. As mentioned above, the exact interior CDW transport computed within neutral density surfaces is around 50% larger than the corresponding transport within potential density surfaces. This may be an important consideration when diagnosing onshore transport of CDW in models of the Antarctic margins, where the CDW supplies almost all of the heat associated with basal melting of the Antarctic ice sheets (*e.g.* Thoma et al., 2008; Nøst et al., 2011).

We conceptually divide the model domain into continental shelf (50 km $< y <$ 150 km), continental slope (150 km $< y <$ 250 km) and deep ocean (250 km $< y <$ 350 km). Figure 5(b) shows that in general the exact and TEM interior transports agree closely over the continental slope. Here the wind stress is close to its maximum, so the overturning is dominated by the mean component $\overline{\psi}$, which may be determined accurately from the mean offshore velocity $\overline{v}$. In the deep ocean the highest-order approximation $\psi^{(\gamma)}_{\mathrm{NDTEM2}}$ is predictably the most accurate approximation to the exact overturning $\psi^{(\gamma)}$, and is comparable to the traditional TEM $\psi^{(\gamma)}_{\mathrm{TEM}}$. On the continental shelf there is almost no difference between the two higher-order TEM approximations $\psi^{(\gamma)}_{\mathrm{NDTEM1}}$ and $\psi^{(\gamma)}_{\mathrm{NDTEM2}}$, though both exhibit approximately half of the error of lowest-order approximation $\psi^{(\gamma)}_{\mathrm{NDTEM0}}$. However, the traditional TEM $\psi^{(\gamma)}_{\mathrm{TEM}}$ underpredicts the onshore transport in the interior by over 50% in places (though the error in the total transport is much smaller). By contrast, the exact and TEM streamfunctions computed based on potential density, $\psi^{(\sigma)}$ and $\psi^{(\sigma)}_{\mathrm{TEM}}$, agree almost perfectly on the continental shelf.

The inaccuracy of $\psi^{(\gamma)}_{\mathrm{TEM}}$ is surprising because in principle the error is $O(\varepsilon^3)$, the same order as the error in $\psi^{(\sigma)}_{\mathrm{TEM}}$. Furthermore, $\psi^{(\gamma)}_{\mathrm{TEM}}$ differs from our NDTEM streamfunctions only in the approximation of the perturbation isopycnal depth z'_0. This suggests that the error associated with approximation (24) is larger than those associated with (25), (23), (22) and (21). In other words, the effective ε is larger in (24). To understand why, consider the evolution of an arbitrary, materially-conserved tracer c,

$$\frac{\mathrm{D}c}{\mathrm{D}t} = \dot{c}, \tag{30}$$

where $\dot{c}$ represents any sources and sinks of c. Potential temperature, salinity and potential density are almost exactly materially conserved: for $c = S$, $c = \theta$ and $c = \sigma$ the source/sink term $\dot{c}$ contains only small explicit and numerical mixing terms. Thus there should be relatively small errors incurred by tracer fluctuations such as σ' in (25) and S' in (14). However, neutral density is not materially conserved due to nonlinearities in the equation of state (see McDougall and Jackett, 2005b), which are particularly pronounced on the continental shelf where there are large isoneutral θ/S gradients (see Figures 1 and 2). These non-conservative terms may enhance the neutral density anomaly γ' via (30), reducing the accuracy of the Taylor expansion in γ' used to derive the isopycnal depth perturbation (24).

4. Discussion

In this article we have shown that the traditional TRM formulation may be extended to provide an efficient and accurate estimate of the volume fluxes between neutral density surfaces,

which we refer to as the Neutral Density Temporal Residual Mean (NDTRM). The novelty in the derivation of the NDTRM lies in the approximation to the isopycnal depth perturbation z_0', which is given in the Boussinesq case by equations (23), (22) and (21), in order of increasing accuracy. These approximations depend only on mean quantities and fluctuations in the potential temperature and salinity, allowing efficient calculation of the corresponding eddy streamfunctions (B.8)–(B.10). However, these approximations to the neutral surface depth perturbation also require knowledge of the neighboring reference cast properties (θ_c,S_c,p_c) at the corresponding neutral density (Jackett and McDougall, 1997). These properties may be determined using the mean potential temperature and salinity via (20). Thus calculation of the NDTRM requires the neutral density to be computed once for each grid box in the model domain, from the time-mean properties of the simulation.

We obtained the neutral densities and cast properties using a modified version of the original neutral density calculation code of Jackett and McDougall (1997). However, this dataset may not in general provide an accurate characterization of approximately neutral surfaces in ocean models, whose solutions may differ substantially from the real ocean's hydrography. As neutral density is defined by a projection along approximately neutral surfaces from the central Pacific, local model biases could dramatically alter the neutral density in other ocean basins. Models with large biases may therefore be better served by defining their own set of neutral density reference casts, based on their own mean states. Our method of calculating the overturning in neutral density coordinates would apply equally well in such situations: one need only replace the cast dataset of Jackett and McDougall (1997) with the model's own "reference casts". Our idealized model test case has been constructed in such a way that the model ocean properties remain close to the hydrography in the northwest Weddell Sea, and thus a neutral density based on the Jackett and McDougall (1997) casts accurately describes the stratification.

Figure 5(b) demonstrates that potential density does not provide a satisfactory approximation to the flux between neutral density surfaces. On the continental shelf, where there are large isoneutral gradients of potential temperature and salinity, the fluxes between potential density surfaces underpredict the shoreward transport in the interior by around 50%. One should also bear in mind that in observations from the Antarctic margins (*e.g.* Thompson and Heywood, 2008) there is no reference pressure that makes the potential density monotonic, so computing fluxes within potential density layers would inevitably lead to a loss of information.

In our tests of the NDTRM we restricted our attention to the simpler TEM, Boussinesq case. This clarifies the presentation whilst still testing the novel aspect of our derivation: the use of the approximate neutral relation (13) to obtain an expression for the isopycnal depth perturbation z_0'. In the non-Boussinesq case it may be more physically relevant to consider the true mass fluxes between neutral density surfaces (Greatbatch and McDougall, 2003). We have simply used thickness averaging for simplicity of presentation and interpretation; it is straightforward to extend our results to the case of mass-weighted fluxes. Our results could also be completely re-cast in terms of Conservative Temperature and Absolute Salinity (McDougall, 2003), which serve as the basis of the latest TEOS-10 equation of state.

The major advantage of the NDTRM is that it may be computed much more quickly than either the "exact" flux within neutral density surfaces or the traditional neutral density TRM (B.12). For the essentially two-dimensional TEM test case described in §3, calculation of the NDTEM streamfunctions $\psi^{(\gamma)}_{\text{NDTEM0}}$, $\psi^{(\gamma)}_{\text{NDTEM1}}$ and $\psi^{(\gamma)}_{\text{NDTEM2}}$ required less than a minute on one core of a modern desktop computer. By contrast, to calculate $\psi^{(\gamma)}$ and $\psi^{(\gamma)}_{\text{TEM}}$ we first computed the neutral density from daily snapshots of θ and S for five years of model output data, which required a total of 24 core-days or around 1440 core-hours. The subsequent calculation of the volume fluxes within the daily neutral density snapshots then required a further 60 core-hours, for a total of around 1500 core-hours. The quasi-two-dimensional nature of the test case exaggerates this contrast slightly, but the difference is still several orders of magnitude.

Our test case in §3 demonstrates that a careful treatment of the overturning circulation is necessary to accurately characterize water mass transformations in regions with large isopycnal gradients of potential temperature and salinity. We illustrated this using an idealized model of the Antarctic margins, where large θ/S gradients are supported across the shelf break in the western Weddell Sea (Thompson and Heywood, 2008) and western Ross Sea (Gordon et al., 2009). Similar configurations arise in the North Atlantic where warm northward surface flows encounter cold shelf water masses, for example in the Greenland Sea (Rudels et al., 2012). The Antarctic Circumpolar Current also supports isopycnal θ/S gradients between the deep northern basins and the Antarctic margins. Combined with the relatively high eddy kinetic energy in this region, this leads to water mass transformations via cabelling on the order of a few Sverdrups (Urakawa and Hasumi, 2012). The TRM streamfunctions derived in this paper could be used to efficiently diagnose water mass transformations in such regions, with improved accuracy over potential density-based calculations.

Acknowledgement

A.L.S.'s and A.F.T.'s work was carried out at the California Institute of Technology under a contract with the National Aeronautics and Space Administration and funded through the President's and Director's Fund Program. The simulations presented herein were conducted using the CITerra computing cluster in the Division of Geological and Planetary Sciences at the California Institute of Technology, and the authors thank the CITerra technicians for facilitating this work. The authors gratefully acknowledge the modeling efforts of the MITgcm team. The authors thank Trevor McDougall and another anonymous reviewer for insightful comments that improved the manuscript.

Appendix A. Approximation of the neutral relation

Here we show that the integrated neutral relation (10) may be approximated using (13) up to third-order accuracy in the small parameter $\Delta \ll 1$. Substituting the Taylor expansion (11) for $\beta(S,\theta,p)$ into (10), we obtain

$$\int_{l_0}^{l_c} \beta(S,\theta,p)\frac{\partial S}{\partial l}\,\mathrm{d}l = \int_{l_0}^{l_c} \Big\{ \beta_m \frac{\partial S}{\partial l} + (S-S_m)\frac{\partial \beta_m}{\partial S_m}\frac{\partial S}{\partial l} + (\theta-\theta_m)\frac{\partial \beta_m}{\partial \theta_m}\frac{\partial S}{\partial l} + (p-p_m)\frac{\partial \beta_m}{\partial p_m}\frac{\partial S}{\partial l} \Big\}\,\mathrm{d}l + O\left(\Delta^3\right). \tag{A.1}$$

The first term on the right-hand side of (A.1) may be integrated directly as

$$\int_{l_0}^{l_c} \beta_m \frac{\partial S}{\partial l}\,\mathrm{d}l = (S_c - S_0)\beta_m, \tag{A.2}$$

whilst the second term integrates exactly to zero,

$$\int_{l_0}^{l_c} (S-S_m)\frac{\partial \beta_m}{\partial S_m}\frac{\partial S}{\partial l}\,\mathrm{d}l = \frac{\partial \beta_m}{\partial S_m}\int_{l_0}^{l_c}\frac{\partial}{\partial l}\left[\tfrac{1}{2}(S-S_m)^2\right]\mathrm{d}l = \frac{\partial \beta_m}{\partial S_m}\left[\tfrac{1}{2}(S-S_m)^2\right]_{l_0}^{l_c} = 0. \tag{A.3}$$

The third term on the right-hand side of (A.1) also integrates to zero. To see this, we write (9) using derivatives with respect to l and apply the Taylor expansion (11) to obtain

$$\beta\frac{\partial S}{\partial l} = \alpha\frac{\partial \theta}{\partial l} \implies \beta_m\frac{\partial S}{\partial l} = \alpha_m\frac{\partial \theta}{\partial l} + O(\Delta). \tag{A.4}$$

Substituting this into the third term on the right-hand side of (A.1), we obtain

$$\int_{l_0}^{l_c} (\theta-\theta_m)\frac{\partial \beta_m}{\partial \theta_m}\frac{\partial S}{\partial l}\,\mathrm{d}l = \frac{\partial \beta_m}{\partial \theta_m}\frac{\alpha_m}{\beta_m}\int_{l_0}^{l_c}(\theta-\theta_m)\frac{\partial \theta}{\partial l}\,\mathrm{d}l = 0, \tag{A.5}$$

where the final equality follows from direct integration, as in (A.3). By applying an analogous procedure to the right-hand side of (10), and applying (A.4) to the last term on the right-hand side of (A.1), we arrive at

$$(S_c - S_0)\beta_m - (\theta_c-\theta_0)\alpha_m = \left(\frac{\partial \alpha_m}{\partial p_m} - \frac{\alpha_m}{\beta_m}\frac{\partial \beta_m}{\partial p_m}\right)\int_{l_0}^{l_c}(p-p_m)\frac{\partial \theta}{\partial l}\,\mathrm{d}l + O\left(\Delta^3\right). \tag{A.6}$$

Jackett and McDougall (1997) showed that the remaining term on the right-hand side of (A.6) is also $O(\Delta^3)$ if potential temperature θ is assumed to depend linearly on pressure p. In fact, if it is possible to write $\theta = \theta_n(p)$ following the neutral coordinate l, then the integral may be written as

$$\int_{l_0}^{l_c}(p-p_m)\frac{\partial \theta}{\partial l}\,\mathrm{d}l = \int_{p_0}^{p_c}(p-p_m)\frac{\mathrm{d}\theta_n}{\mathrm{d}p}\,\mathrm{d}p. \tag{A.7}$$

Then, posing a Taylor expansion of $\theta_n(p)$ about $p = p_m$ yields

$$\frac{\mathrm{d}\theta_n}{\mathrm{d}p} = \left.\frac{\mathrm{d}\theta_n}{\mathrm{d}p}\right|_{p=p_m} + (p-p_m)\left.\frac{\mathrm{d}^2\theta_n}{\mathrm{d}p^2}\right|_{p=p_m} + O\left(\Delta^2\right). \tag{A.8}$$

Substituting (A.8) into (A.7) and evaluating the integral, it follows that the right-hand side of (A.6) is $O(\Delta^3)$.

However, in general it may not be the case that we can write $\theta = \theta_n(p)$ along the neutral path, *i.e.* the path may encounter multiple values of potential temperature θ at the same pressure p. In this case, we start by writing $p = p(l)$ and $\theta = \theta(l)$ along the neutral path. We note that the in general mid-value of the pressure along the path is not equal to the pressure mid-way along the path, $p_m \neq p(l_m)$. However, the difference between these pressures is $O(\Delta^2)$:

$$\begin{aligned} p_m - p(l_m) &= \tfrac{1}{2}(p(l_0)+p(l_c)) - p\left(l_0 + \tfrac{1}{2}(l_c-l_0)\right) \\ &= \tfrac{1}{2}\left[2p(l_0) + (l_c-l_0)\frac{\partial p}{\partial l}(l_0) + O(\Delta^2)\right] \\ &\quad - \left[p(l_0) + \tfrac{1}{2}(l_c-l_0)\frac{\partial p}{\partial l}(l_0) + O(\Delta^2)\right] \\ &= 0 + O(\Delta^2). \end{aligned} \tag{A.9}$$

Thus, we may write the integral on the right-hand side of (A.6) as

$$\int_{l_0}^{l_c}(p-p_m)\frac{\partial \theta}{\partial l}\,\mathrm{d}l = \int_{l_0}^{l_c}(p-p(l_m))\frac{\partial \theta}{\partial l}\,\mathrm{d}l + O\left(\Delta^3\right). \tag{A.10}$$

Then, expanding $p(l)$ and $\partial\theta/\partial l$ as Taylor series about $l = l_m$, it may be shown that the expressions in (A.10) are $O(\Delta^3)$, and thus the approximate neutral relation (13) is accurate up to $O(\Delta^3)$.

Appendix B. The NDTRM streamfunction in explicit form

In this Appendix we give explicit expressions for the NDTRM eddy streamfunction, both in the general case of an arbitrary pressure distribution, and in the Boussinesq case.

Appendix B.1. General case

Equation (19) for the isopycnal depth perturbations can be written more succinctly using coefficients for the perturbation salinity S', potential temperature θ' and pressure p' in the numerator,

$$\mathcal{B} = \overline{\beta}_m - \tfrac{1}{2}\frac{\partial \overline{\beta}_m}{\partial \overline{S}_m}\left(S_c - \overline{S}\right) + \tfrac{1}{2}\frac{\partial \overline{\alpha}_m}{\partial \overline{S}_m}\left(\theta_c - \overline{\theta}\right) \tag{B.1a}$$

$$\mathcal{A} = \overline{\alpha}_m + \tfrac{1}{2}\frac{\partial \overline{\beta}_m}{\partial \overline{\theta}_m}\left(S_c - \overline{S}\right) - \tfrac{1}{2}\frac{\partial \overline{\alpha}_m}{\partial \overline{\theta}_m}\left(\theta_c - \overline{\theta}\right) \tag{B.1b}$$

$$\mathcal{G} = -\tfrac{1}{2}\frac{\partial \overline{\beta}_m}{\partial \overline{p}_m}\left(S_c - \overline{S}\right) + \tfrac{1}{2}\frac{\partial \overline{\alpha}_m}{\partial \overline{p}_m}\left(\theta_c - \overline{\theta}\right). \tag{B.1c}$$

We also denote the denominator as

$$\begin{aligned} \mathcal{N}^2 = \Big\{ & \overline{S}_z\overline{\beta}_m - \overline{\theta}_z\overline{\alpha}_m \\ & - \left(S_c - \overline{S}\right)\left[\tfrac{1}{2}\overline{S}_z\frac{\partial \overline{\beta}_m}{\partial \overline{S}_m} + \tfrac{1}{2}\overline{\theta}_z\frac{\partial \overline{\beta}_m}{\partial \overline{\theta}_m} + \tfrac{1}{2}\overline{p}_z\frac{\partial \overline{\beta}_m}{\partial \overline{p}_m}\right] \\ & + \left(\theta_c - \overline{\theta}\right)\left[\tfrac{1}{2}\overline{S}_z\frac{\partial \overline{\alpha}_m}{\partial \overline{S}_m} + \tfrac{1}{2}\overline{\theta}_z\frac{\partial \overline{\alpha}_m}{\partial \overline{\theta}_m} + \tfrac{1}{2}\overline{p}_z\frac{\partial \overline{\alpha}_m}{\partial \overline{p}_m}\right] \Big\} \end{aligned} \tag{B.2}$$

where the notation $\mathcal{N}^2$ has been chosen because the denominator is approximately proportional to the density stratification. These definitions allow us to rewrite (19) as

$$z_0' = -\frac{\mathcal{B}S' - \mathcal{A}\theta' + \mathcal{G}p'}{\mathcal{N}^2} + O\left(\Delta^3, \varepsilon^2\right), \tag{B.3}$$

and thus the eddy streamfunction (4c) is

$$\begin{aligned}\boldsymbol{\Psi}^\star =& \frac{\mathcal{B}\overline{\boldsymbol{u}'S'} - \mathcal{A}\overline{\boldsymbol{u}'\theta'} + \mathcal{G}\overline{\boldsymbol{u}'p'}}{\mathcal{N}^2} \\ &- \frac{\frac{1}{2}\overline{\boldsymbol{u}}_z}{\mathcal{N}^4}\Big\{ \mathcal{B}^2\overline{S'^2} + \mathcal{A}^2\overline{\theta'^2} + \mathcal{G}^2\overline{p'^2} \\ &- 2\mathcal{B}\mathcal{A}\overline{S'\theta'} + 2\mathcal{B}\mathcal{G}\overline{S'p'} - 2\mathcal{A}\mathcal{G}\overline{\theta'p'} \Big\} \\ &+ O\left(\varepsilon\Delta^3, \varepsilon^3\right). \end{aligned} \tag{B.4}$$

Appendix B.2. Boussinesq case

Under the Boussinesq approximation (21) there is no pressure perturbation coefficient $\mathcal{G} = 0$, and the coefficients associated with the salinity and potential temperature perturbations are identical to (B.1a) and (B.1b). The denominator is slightly modified to

$$\begin{aligned}\mathcal{N}^2 = \Big\{ & \overline{S}_z\overline{\beta}_m - \overline{\theta}_z\overline{\alpha}_m \\ &- \left(S_c - \overline{S}\right)\left[\tfrac{1}{2}\overline{S}_z\frac{\partial\overline{\beta}_m}{\partial\overline{S}_m} + \tfrac{1}{2}\overline{\theta}_z\frac{\partial\overline{\beta}_m}{\partial\overline{\theta}_m} + \tfrac{1}{2}\frac{\partial\overline{\beta}_m}{\partial\overline{z}_m}\right] \\ &+ \left(\theta_c - \overline{\theta}\right)\left[\tfrac{1}{2}\overline{S}_z\frac{\partial\overline{\alpha}_m}{\partial\overline{S}_m} + \tfrac{1}{2}\overline{\theta}_z\frac{\partial\overline{\alpha}_m}{\partial\overline{\theta}_m} + \tfrac{1}{2}\frac{\partial\overline{\alpha}_m}{\partial\overline{z}_m}\right] \Big\}. \end{aligned} \tag{B.5}$$

The eddy streamfunction is again given by (B.4). If we further approximate the isopycnal depth perturbations as (22) then we the coefficients reduce to

$$\mathcal{A} = \overline{\alpha}_m, \quad \mathcal{B} = \overline{\beta}_m, \quad \mathcal{N}^2 = \overline{S}_z\overline{\beta}_m - \overline{\theta}_z\overline{\alpha}_m. \tag{B.6}$$

Finally, under the most severe approximation (23), the coefficients become

$$\mathcal{A} = \overline{\alpha}, \quad \mathcal{B} = \overline{\beta}, \quad \mathcal{N}^2 = \overline{S}_z\overline{\beta} - \overline{\theta}_z\overline{\alpha}. \tag{B.7}$$

As above, $\overline{\alpha}$ and $\overline{\beta}$ are shorthands for $\alpha(\overline{S}, \overline{\theta}, \overline{p})$ and $\beta(\overline{S}, \overline{\theta}, \overline{p})$ respectively.

Appendix B.3. TEM streamfunctions

In the TEM test case described in §3m the mean $\overline{\bullet}$ should be interpreted as a time- and alongshore-average. The term proportional to $\overline{\boldsymbol{u}}_z$ in (B.4) can be neglected because in a re-entrant channel it is not possible to support a cross-slope geostrophic transport. In this case (B.4) reduces to

$$\psi^{\star(\gamma)}_{\text{NDTEM2}} = \frac{\mathcal{B}\overline{v'S'} - \mathcal{A}\overline{v'\theta'}}{\mathcal{N}^2} + O\left(\varepsilon\Delta^3, \varepsilon^3\right). \tag{B.8}$$

At each point in our computational domain we calculate the coefficients $\mathcal{B}$, $\mathcal{A}$ and $\mathcal{N}^2$ using each of the four neighboring reference casts, and then use the weighted average of each coefficient to calculate the streamfunction via (B.8). Additionally neglecting the $O(\varepsilon^2\Delta)$ terms in (B.8) yields

$$\psi^{\star(\gamma)}_{\text{NDTEM1}} = \frac{\overline{\beta}_m\overline{v'S'} - \overline{\alpha}_m\overline{v'\theta'}}{\overline{\beta}_m\overline{S}_z - \overline{\alpha}_m\overline{\theta}_z} + O\left(\varepsilon\Delta^3, \varepsilon^3, \varepsilon^2\Delta\right). \tag{B.9}$$

Further approximating (B.9) by replacing the midpoint saline contraction and thermal expansion coefficients, $\overline{\beta}_m$ and $\overline{\alpha}_m$, with their values at the parcel, $\overline{\beta}$ and $\overline{\alpha}$, simplifies (B.9) to

$$\psi^{\star(\gamma)}_{\text{NDTEM0}} = \frac{\overline{\beta}\,\overline{v'S'} - \overline{\alpha}\,\overline{v'\theta'}}{\overline{\beta}\,\overline{S}_z - \overline{\alpha}\,\overline{\theta}_z} + O\left(\varepsilon\Delta^2, \varepsilon^3, \varepsilon^2\Delta\right). \tag{B.10}$$

Recall that $\overline{\alpha}$ and $\overline{\beta}$ are shorthands for $\alpha(\overline{S}, \overline{\theta}, \overline{p})$ and $\beta(\overline{S}, \overline{\theta}, \overline{p})$ respectively.

For the purpose of comparison we also employ the straightforward TRM form of the eddy streamfunction (McIntosh and McDougall, 1996) using potential density,

$$\psi^{\star(\sigma)}_{\text{TEM}} = \frac{\overline{v'\sigma'}}{\overline{\sigma}_z} + O\left(\varepsilon^3\right), \tag{B.11}$$

and using neutral density,

$$\psi^{\star(\gamma)}_{\text{TEM}} = \frac{\overline{v'\gamma'}}{\overline{\gamma}_z} + O\left(\varepsilon^3\right). \tag{B.12}$$

These may be derived by substituting expressions (25) and (24) for the isopycnal depth perturbation into (4c).

References

Ballarotta, M., Drijfhout, S., Kuhlbrodt, T., Döös, K., 2013. The residual circulation of the Southern Ocean: Which spatio-temporal scales are needed? Ocean Modell. 64, 46–55.

de Szoeke, R. A., Springer, S. R., Oxilia, D. M., 2000. Orthobaric density: A thermodynamic variable for ocean circulation studies. J. Phys. Oceanogr. 30 (11), 2830–2852.

Döös, K., Nilsson, J., Nycander, J., Brodeau, L., Ballarotta, M., 2012. The World Ocean Thermohaline Circulation. J. Phys. Oceanogr. 42 (9), 1445–1460.

Döös, K., Webb, D. J., 1994. The Deacon cell and the other meridional cells of the Southern Ocean. J. Phys. Oceanogr. 24, 429–429.

Eden, C., Willebrand, J., 1999. Neutral density revisited. Deep Sea Res. Pt. II 46 (1), 33–54.

Fox-Kemper, B., Menemenlis, D., 2008. Can large eddy simulation techniques improve mesoscale rich ocean models? Geophys. Monogr. Ser. 177, 319–338.

Gill, A. E., 1973. Circulation and bottom water production in the Weddell Sea. Deep-Sea Res. 20 (2), 111–140.

Gordon, A. L., Orsi, A. H., Muench, R., Huber, B. A., Zambianchi, E., Visbeck, M., 2009. Western Ross Sea continental slope gravity currents. Deep-Sea Res. Pt. II 56 (13), 796–817.

Greatbatch, R. J., McDougall, T. J., 2003. The non-Boussinesq temporal residual mean. J. Phys. Oceanogr. 33 (6), 1231–1239.

Haidvogel, D. B., Arango, H., Budgell, W. P., Cornuelle, B. D., Curchitser, E., Di Lorenzo, E., Fennel, K., Geyer, W. R., Hermann, A. J., Lanerolle, L., 2008. Ocean forecasting in terrain-following coordinates: Formulation and skill assessment of the Regional Ocean Modeling System. J. Comp. Phys. 227 (7), 3595–3624.

Hallberg, R., Rhines, P., 1996. Buoyancy-driven circulation in an ocean basin with isopycnals intersecting the sloping boundary. J. Phys. Oceanogr. 26 (6), 913–940.

Hill, C., Ferreira, D., Campin, J. M., Marshall, J., Abernathey, R., Barrier, N., 2012. Controlling spurious diapycnal mixing in eddy-resolving height-coordinate ocean models — Insights from virtual deliberate tracer release experiments. Ocean Modelling 45, 14–26.

Hirst, A. C., Jackett, D. R., McDougall, T. J., 1996. The meridional overturning cells of a world ocean model in neutral density coordinates. J. Phys. Oceanogr. 26 (5), 775–791.

Jackett, D. R., McDougall, T. J., 1997. A neutral density variable for the world's oceans. J. Phys. Oceanogr. 27 (2), 237–263.

Johns, W. E., Baringer, M. O., Beal, L. M., Cunningham, S. A., Kanzow, T., Bryden, H. L., Hirschi, J. J. M., Marotzke, J., Meinen, C. S., Shaw, B., 2011. Continuous, array-based estimates of Atlantic Ocean heat transport at 26.5 N. J. Climate 24 (10), 2429–2449.

Large, W. G., Yeager, S. G., 2009. The global climatology of an interannually varying air–sea flux data set. Climate Dynam. 33 (2), 341–364.

Lumpkin, R., Speer, K., 2007. Global ocean meridional overturning. J. Phys. Oceanogr. 37 (10), 2550–2562.

Marshall, J., Adcroft, A., Hill, C., Perelman, L., Heisey, C., 1997a. A finite-volume, incompressible Navier Stokes model for studies of the ocean on parallel computers. J. Geophys. Res. 102, 5753–5766.

Marshall, J., Hill, C., Perelman, L., Adcroft, A., 1997b. Hydrostatic, quasi-hydrostatic, and nonhydrostatic ocean modeling. J. Geophys. Res. 102, 5733–5752.

Marshall, J., Radko, T., 2003. Residual-mean solutions for the Antarctic Circumpolar Current and its associated overturning circulation. J. Phys. Oceanogr. 33 (11), 2341–2354.

McDougall, T. J., 1987. Neutral surfaces. J. Phys. Oceanogr. 17 (11), 1950–1964.

McDougall, T. J., 2003. Potential enthalpy: A conservative oceanic variable for evaluating heat content and heat fluxes. J. Phys. Oceanogr. 33 (5), 945–963.

McDougall, T. J., Jackett, D. R., 2005a. An assessment of orthobaric density in the global ocean. J. Phys. Oceanogr. 35 (11), 2054–2075.

McDougall, T. J., Jackett, D. R., 2005b. The material derivative of neutral density. J. Mar. Res. 63 (1), 159–185.

McDougall, T. J., Jackett, D. R., 2007. The thinness of the ocean in s-θ-p space and the implications for mean diapycnal advection. J. Phys. Oceanogr. 37 (6), 1714–1732.

McDougall, T. J., McIntosh, P. C., 1996. The temporal-residual-mean velocity. Part I: Derivation and the scalar conservation equations. J. Phys. Oceanogr. 26 (12), 2653–2665.

McDougall, T. J., McIntosh, P. C., 2001. The temporal-residual-mean velocity. Part II: Isopycnal interpretation and the tracer and momentum equations. J. Phys. Oceanogr. 31 (5), 1222–1246.

McIntosh, P. C., McDougall, T. J., 1996. Isopycnal averaging and the residual mean circulation. J. Phys. Oceanogr. 26 (8), 1655–1660.

Nøst, O. A., Biuw, M., Tverberg, V., Lydersen, C., Hattermann, T., Zhou, Q., Smedsrud, L. H., Kovacs, K. M., 2011. Eddy overturning of the Antarctic Slope Front controls glacial melting in the Eastern Weddell Sea. J. Geophys. Res 116, C11014.

Nurser, A. J. G., Lee, M. M., 2004a. Isopycnal averaging at constant height. Part I: The formulation and a case study. J. Phys. Oceanogr. 34 (12), 2721–2739.

Nurser, A. J. G., Lee, M. M., 2004b. Isopycnal averaging at constant height. Part II: Relating to the residual streamfunction in Eulerian space. J. Phys. Oceanogr. 34 (12), 2740–2755.

Plumb, R. A., Ferrari, R., 2005. Transformed Eulerian-mean theory. Part I: Nonquasigeostrophic theory for eddies on a zonal-mean flow. J. Phys. Oceanogr. 35 (2), 165–174.

Prather, M. J., 1986. Numerical advection by conservation of second-order moments. J. Geophys. Res. 91 (D6), 6671–6681.

Rudels, B., Korhonen, M., Budéus, G., Beszczynska-Möller, A., Schauer, U., Nummelin, A., Quadfasel, D., Valdimarsson, H., 2012. The East Greenland Current and its impacts on the Nordic Seas: observed trends in the past decade. IICES J. Mar. Sci. 69 (5), 841–851.

Schmidt, G. A., Bitz, C. M., Mikolajewicz, U., Tremblay, L., 2004. Ice–ocean boundary conditions for coupled models. Ocean Modell. 7 (1), 59–74.

Shchepetkin, A. F., McWilliams, J. C., 2005. The regional oceanic modeling system (ROMS): a split-explicit, free-surface, topography-following-coordinate oceanic model. Ocean Modell. 9 (4), 347–404.

Stewart, A. L., Thompson, A. F., 2015. Eddy-mediated transport of warm Circumpolar Deep Water across the Antarctic Shelf Break. Geophys. Res. Lett. 42 (2), 432–440.

Talley, L. D., 2013. Closure of the global overturning circulation through the Indian, Pacific, and Southern Oceans: Schematics and transports. Oceanography 26 (1), 80–97.

Tamura, T., Ohshima, K. I., Nihashi, S., 2008. Mapping of sea ice production for Antarctic coastal polynyas. Geophys. Res. Lett. 35 (7).

Thoma, M., Jenkins, A., Holland, D., Jacobs, S., 2008. Modelling circumpolar deep water intrusions on the Amundsen Sea continental shelf, Antarctica. Geophys. Res. Lett. 35 (18), L18602.

Thompson, A. F., Heywood, K. J., 2008. Frontal structure and transport in the northwestern Weddell Sea. Deep-Sea Res. Pt. I 55 (10), 1229–1251.

Urakawa, L. S., Hasumi, H., 2012. Eddy-resolving model estimate of the cabbeling effect on the water mass transformation in the Southern Ocean. J. Phys. Oceanogr. 42 (8), 1288–1302.

Wolfe, C. L., 2014. Approximations to the ocean's residual circulation in arbitrary tracer coordinates. Ocean Modell. 75, 20–35.

Young, W. R., 2012. An exact thickness-weighted average formulation of the Boussinesq equations. J. Phys. Oceanogr. 42 (5), 692–707.

Zika, J. D., England, M. H., Sijp, W. P., 2012. The ocean circulation in thermohaline coordinates. J. Phys. Oceanogr. 42 (5), 708–724.

Zika, J. D., Le Sommer, J., Dufour, C. O., Molines, J.-M., Barnier, B., Brasseur, P., Dussin, R., Penduff, T., Iudicone, D., Lenton, A., 2013. Vertical eddy fluxes in the Southern Ocean. J. Phys. Oceanogr. 43 (5), 941–955.